A Computational Study of S_N2 Reactions: $CH_3X + F^- \rightarrow CH_3F + X^-$

X = F, Cl, CN, OH, SH, NH_2

By

Barnik Pal (2019/UG/010) & **Sejuti Mukherjee** (2019/UG/027)

Indian Association for the Cultivation of Science

- **Introduction:**

Bimolecular nucleophilic substitution (S_N2) reactions at carbon centers are among the most intensely studied of all chemical reactions. The class of reactions, exemplified by:

$$CH_3X + F^- \rightarrow CH_3F + X^-, \quad \text{where X= (F, Cl, CN, OH, SH } NH_2)$$

has been investigated by an exceptional array of kinetic experiments, ab-initio quantum and semiclassical dynamical methods and trajectory simulations, statistical mechanical studies, ab-initio and density functional structural analyses, and electron-transfer studies [1].

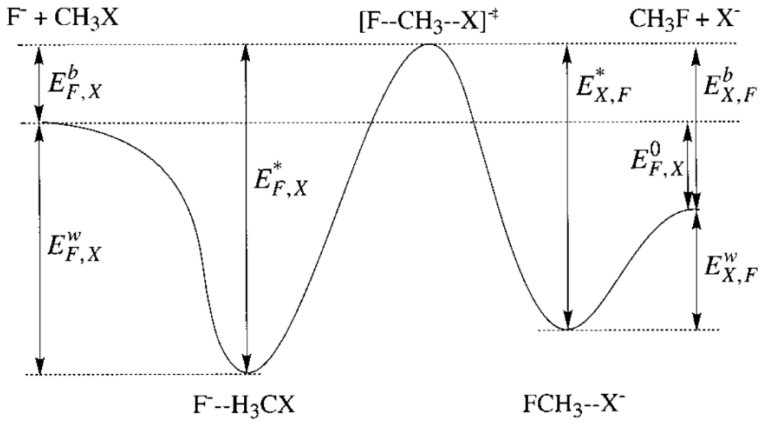

Figure 1. Energy diagram for a prototypical gas-phase S_N2 reaction. Note the double well with two minima corresponding to ion-molecule complexes.

Early research was restricted to solution phase chemistry, but the advent of flowing afterglow and ion-cyclotron resonance techniques in the 1970s initiated a deep interest in the fundamental gas-phase chemistry of S_N2 reactions. It was discovered that gas-phase S_N2 reactions generally exhibit a double-well potential with a central barrier, as depicted in Figure1 for the reaction of F^- and CH_3X.

- **Aim of the study:**

1. To find the relative stabilities of the reactant and products with HF, DFT (B3LYP) and MP2 at 6-31+G(d) basis set.
2. Comparison of reaction enthalpies (ΔH) of the aforesaid S_N2 reactions with experimental numbers.
3. To find the forward and backward barrier of the reactions at MP2/6-31+G(d) level.

- **Computational methods:**

The methods employed in this study are the Hartree-Fock (HP), Møller–Plesset perturbation theory (MP2) and the B3LYP density functional. The B3LYP functional is a combination of the hybrid three-parameter Becke exchange functional and the Lee-Yang-Parr correlation functional (LYP). The basis set used here is the 6-31+G(d) basis set. 6-31+G(d) designates the 6-31G basis set supplemented by diffuse functions and one set of d-functions. All computations were performed using the GAUSSIAN 09W [5] computational package, supported by GaussView 6 and Avogadro software for structure visualization.

- **Reaction enthalpies at different levels of theory:**

For the given S_N2 class of reactions, we optimized the reactant and product structures of all the reactions with HF, DFT (B3LYP) and MP2 at 6-31+G(d) basis set. The results are published below [2].

1. **$CH_3F + F^- \rightarrow CH_3F + F^-$**

In this identity S_N2 reaction, F^- act as both a nucleophile and a leaving group. The structures for the $CH_3F + F^-$ reaction are detailed in Figure 2. Because this is an identity exchange reaction, there is only one distinct ion-molecule complex.

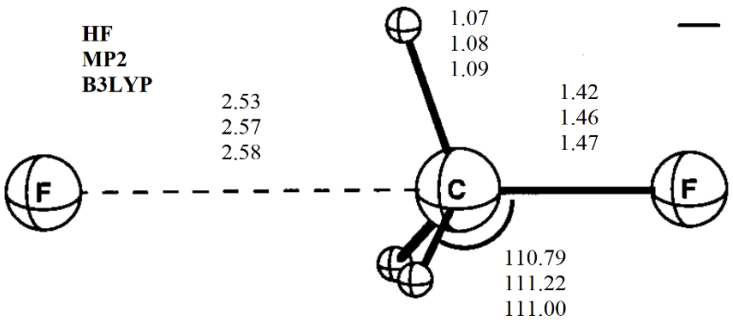

◄**Figure 2**: Geometries of the ion-molecule complex for the reaction $CH_3F + F^-$. All bond distances are in Å and bond angles in degrees. The ion-molecule complex is C_{3V} symmetry.

Finally, the energetic quantities associated with this reaction are considered, as listed in Table 1.

Table 1: Energetics of the reaction $CH_3F + F^-$

	E_{prod} (Ha)	E_{reac} (Ha)	ΔH (kcal mol^{-1})
HF	-238.483	-238.483	0.0
MP2	-238.999	-238.999	0.0
B3LYP	-239.632	-239.633	0.001

2. **$CH_3Cl + F^- \rightarrow CH_3F + Cl^-$**

This in a non-identity S_N2 reaction with Cl^- as the leaving group. The structures for the $CH_3Cl + F^-$ reaction are detailed in Figure 3. Finally, the energetic quantities associated with this reaction are considered, as listed in Table 2.

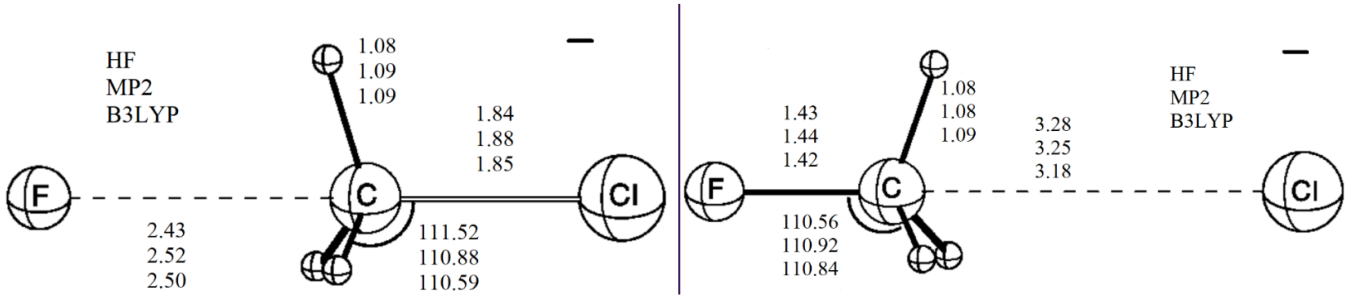

Figure 3: Geometries of the ion-molecule complex of reactants and products for the reaction $CH_3Cl + F^-$. All bond distances are in Å and bond angles in degrees. All structures are C_{3V} symmetry.

Table 2: Energetics of the reaction $CH_3Cl + F^-$

	E_{prod} (Ha)	E_{reac} (Ha)	ΔH (kcal mol^{-1})
HF	-598.595	-598.535	-37.329
MP2	-599.039	-599.005	-21.606
B3LYP	-600.039	-599.998	-25.628

3. **$CH_3CN + F^- \rightarrow CH_3F + CN^-$**

The reaction of acetonitrile with F^- anion has been studied and the we have included the optimized structures of the reactants and products of this reaction in Figure 4.

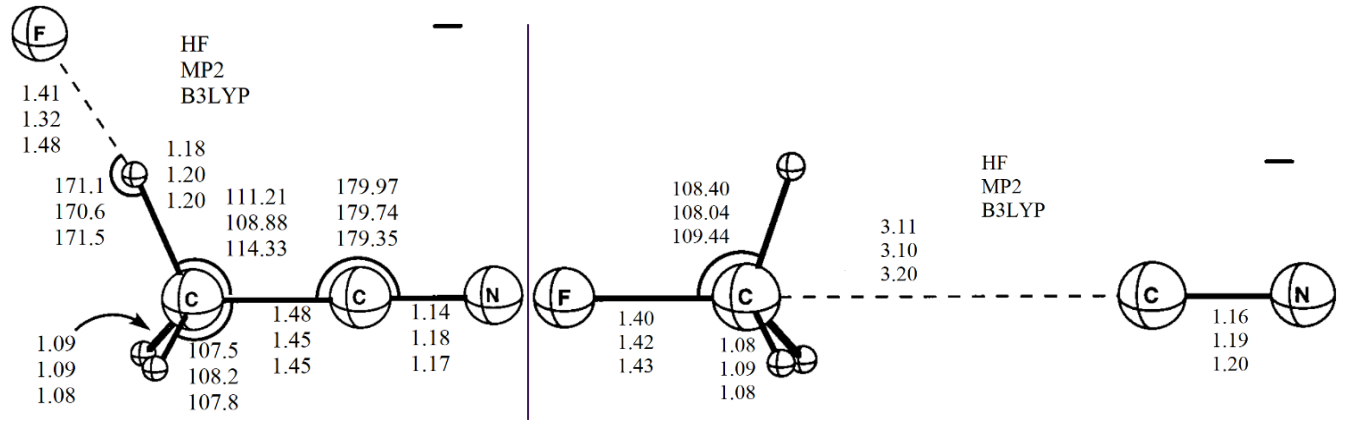

Figure 4: Geometries of the ion-molecule complex of reactants and products for the reaction $CH_3CN + F^-$. All bond distances are in Å and bond angles in degrees. The reactant is C_S symmetry while the product is C_{3V} symmetry.

The computed energetics of this reaction are tabulated in Table 3. In this reaction, we observed a discrepancy between the calculations done by HF theory and the MP2/B3LYP functionals. Inclusion of proper diffused and/or polarized basis sets could have yielded better results.

Table 3: Energetics of the reaction $CH_3CN + F^-$

	E_{prod} (Ha)	E_{reac} (Ha)	ΔH (kcal mol^{-1})
HF	-231.371	-231.377	3.566
MP2	-231.971	-232.003	20.165
B3LYP	-232.629	-232.660	19.278

4. **$CH_3OH + F^- \rightarrow CH_3F + OH^-$**

The reaction of acetonitrile with F^- anion has been studied and the we have included the optimized structures of the reactants and products of this reaction in Figure 5.

The $CH_3OH + F^-$ system is the first encountered here without a reactant complex for backside attack, rather a CH3OH.F^- complex with a very strong semi-covalent bond to the acidic hydroxyl hydrogen. In contrast, the product complex, $FCH_3.OH^-$, is a typical ion-dipole adduct, albeit with a loose C-O-H bending mode.

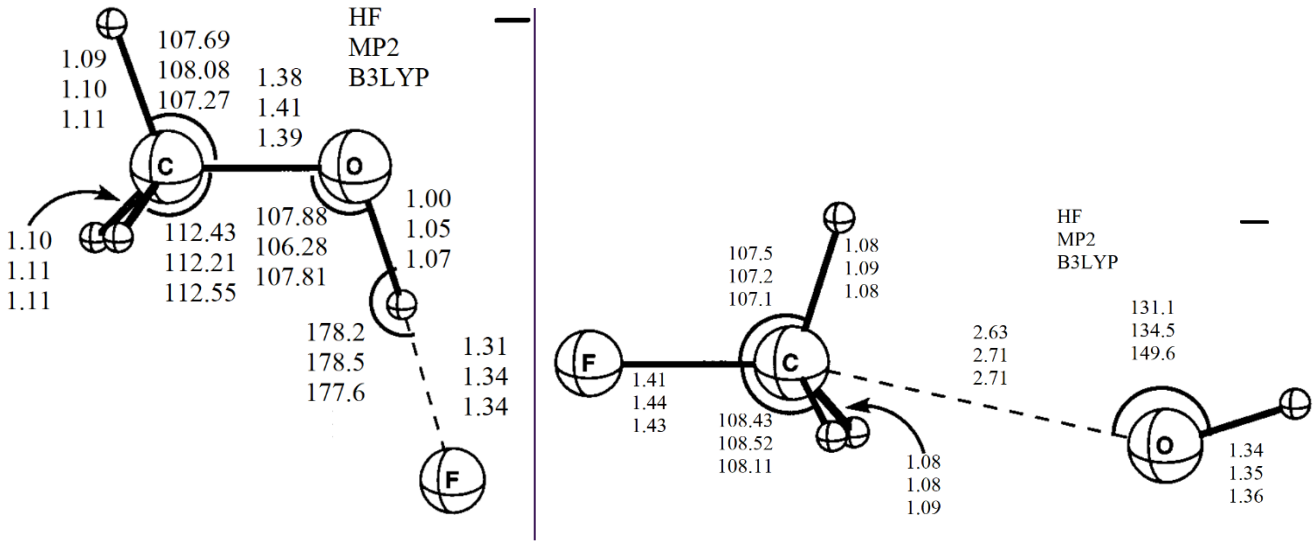

Figure 5: Geometries of the ion-molecule complex of reactants and products for the reaction $CH_3OH + F^-$. All bond distances are in Å and bond angles in degrees. All structures are C_S symmetry.

The computed energetics of this reaction are tabulated in Table 4.

Table 4: Energetics of the reaction $CH_3OH + F^-$

	E_{prod} (Ha)	E_{reac} (Ha)	ΔH (kcal mol^{-1})
HF	-214.441	-214.500	36.927
MP2	-214.965	-215.027	38.657
B3LYP	-215.570	-215.633	39.455

5. **$CH_3SH + F^- \rightarrow CH_3F + SH^-$**

The reaction of acetonitrile with F^- anion has been studied and the we have included the optimized structures of the reactants and products of this reaction in Figure 6.

The $CH_3SH + F^-$ surface has the same topology as for $CH_3OH + F^-$, but exhibits greater extremes. We find no evidence of a backside reactant complex, only a $CH_3SH.F^-$adduct with a high binding energy and massive charge transfer (more like CH_3S^-.HF). The energetics of this reaction are listed in Table 5.

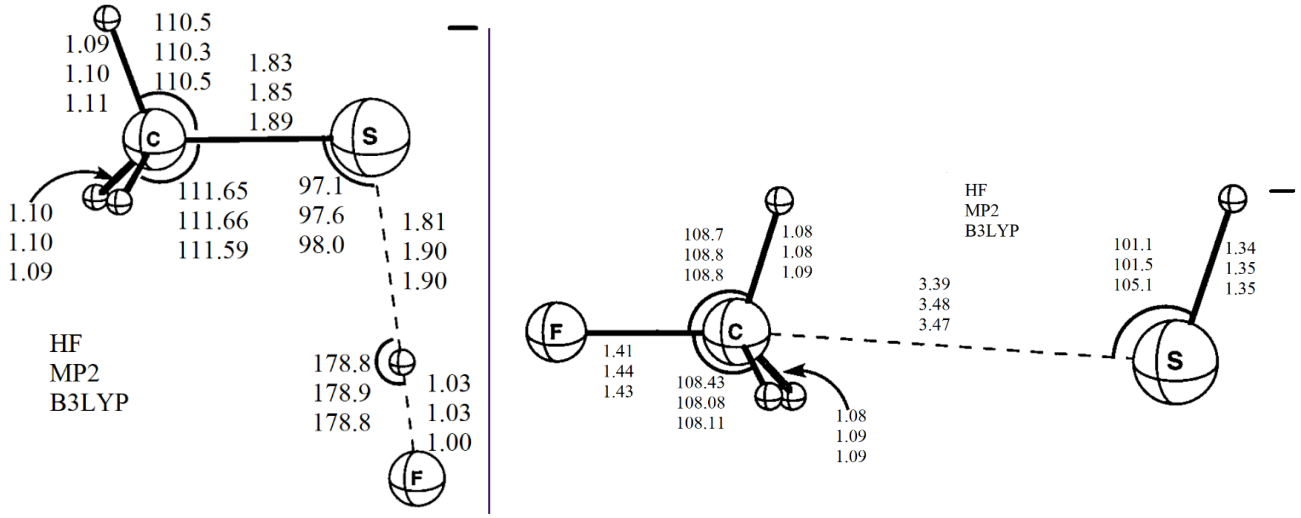

Figure 5: Geometries of the ion-molecule complex of reactants and products for the reaction $CH_3SH + F^-$. All bond distances are in Å and bond angles in degrees. All structures are C_S symmetry.

Table 5: Energetics of the reaction $CH_3SH + F^-$

	E_{prod} (Ha)	E_{reac} (Ha)	ΔH (kcal mol^{-1})
HF	-537.163	-537.175	8.070

MP2	-537.598	-537.631	20.759
B3LYP	-538.591	-538.617	15.970

6. **$CH_3NH_2 + F^- \rightarrow CH_3F + NH_2^-$**

The $CH_3NH_2 + F^-$ reaction has similar characteristics to its methanol and methanethiol counterparts: a backside reactant complex is precluded by a strong frontside adduct involving hydrogen bonding to a single, acidic proton, except now in C_1 symmetry and with a much smaller binding energy; and the product complex, of electrostatic type, has a nonlinear heavy atom framework with facile, large amplitude distortions. The energetics of this reaction are listed in Table 6.

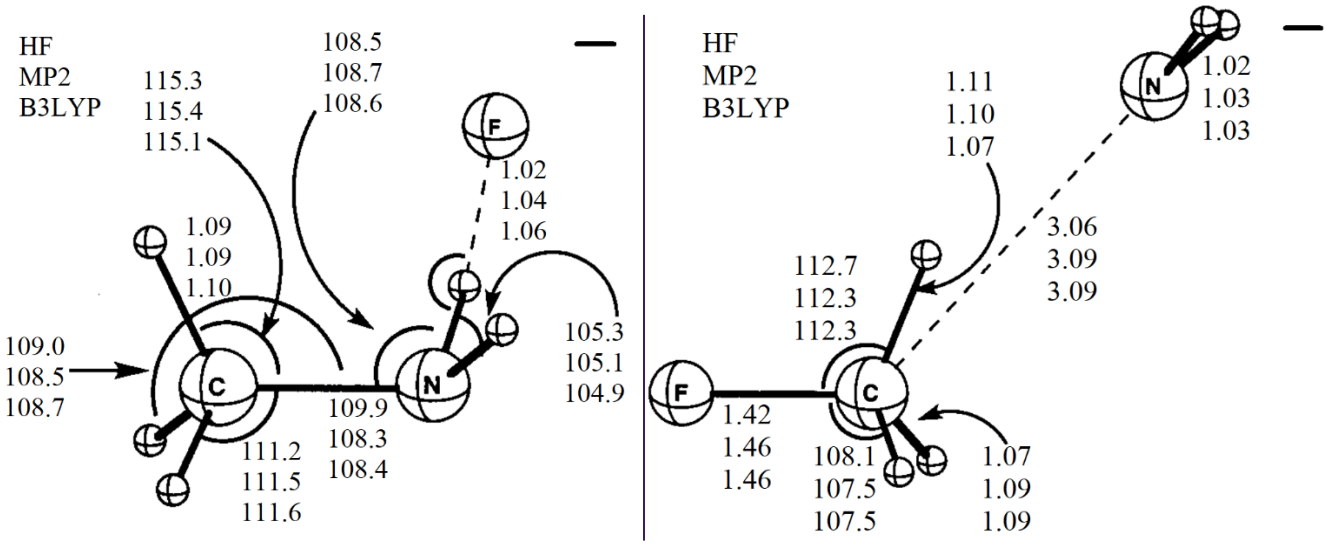

Figure 6: Geometries of the ion-molecule complex of reactants and products for the reaction $CH_3NH_2 + F^-$. All bond distances are in Å and bond angles in degrees. The reactant is C_1 symmetry while the product is C_S symmetry.

Table 6: Energetics of the reaction $CH_3NH_2 + F^-$

	E_{prod} (Ha)	E_{reac} (Ha)	ΔH (kcal mol^{-1})
HF	-194.581	-194.655	46.152
MP2	-195.084	-195.165	50.767
B3LYP	-195.672	-195.749	47.909

- **Comparing computed ΔH with experimental ΔH:**

A statistical characterization of the energetic data is given below in Table 2. We calculated the average absolute deviations w.r.t experimental gas-phase data for each level of theory. We noted the largest disparity in MP2/6-31+(d) level of theory with δ_{ABS} as large as **18.4**. This clearly indicates that out of all three MP2/6-31+(d) is least favored with greatest scatter about ΔH_{exp}.

On the other hand, HF/631+G(d) performs quite well with δ_{ABS} = **11.2**. In general, considering qualitative topology, and both maximum and average errors, B3LYP is the only one which may be considered to give adequate energetics for these S_N2 systems. In our case, it does not perform very well, with δ_{ABS} = **16.1** and the values are scattered about the experimental numbers.

This is probably due to the use of 6-31+G(d) basis set which is a valence double-zeta polarized basis set. Correlation-consistent or Polarization-consistent basis sets such as aug-cc-pVDZ are more appropriate for energetic calculations involving correlated wavefunctions.

Table 7: Average Absolute Deviations (δ_{ABS}) in kcal mol^{-1} of Energetic Quantities w.r.t Experimental Data

	HF/6-31+G(d)		**MP2/6-31+G(d)**		**B3LYP/6-31+G(d)**		**ΔH_{exp} (Experimental)** [2]
	ΔH_{HF}	*δ_{ABS} from* ΔH_{exp}	ΔH_{MP2}	*δ_{ABS} from* ΔH_{exp}	ΔH_{B3LYP}	*δ_{ABS} from* ΔH_{exp}	
F	0	0	0	0	0	0	0
Cl	-37.32	6.12	-21.6	9.6	-25.62	5.58	-31.2
CN	3.56	1.44	20.16	15.16	19.27	14.27	5
OH	36.92	17.22	38.65	18.95	39.45	19.75	19.7
SH	8.07	22.77	20.75	35.45	15.97	30.67	-14.7
NH_2	46.15	8.65	50.76	13.26	47.9	10.4	37.5
δ_{ABS} Average		**11.240**		**18.484**		**16.134**	**0**

Note: All values are in **kcal mol^{-1}** units.

- **Activation energies at MP2/6-31+G(d) level:**

In order to calculate the Activation barriers of the aforesaid S_N2 reactions, it is necessary to obtain an optimized transition state (TS) for each of the reactions.

1. **TS optimization:**

The transition state is mathematically defined as a saddle point on this multidimensional molecular potential energy surface (PES). At such a point the first derivative of the potential with respect to any nuclear coordinate is zero, and the second derivative is positive for all but one coordinate.

We optimized the TS for our reactions using **Synchronous Transit-Guided Quasi-Newton** (STQN) methods available in Gaussian software. This method uses a quadratic synchronous transit approach to get closer to the quadratic region of the transition state and then uses a quasi-Newton or eigenvector-following algorithm to complete the optimization.

We used the **QST3** method which requires three molecule specifications: the reactants, the products, and an initial structure for the transition state, in that order. *The order of the atoms must be identical within all molecule specifications.*

The following set of figures illustrate the structures obtained by using the aforesaid methods:

Note: All bond distances are in Å and bond angles in degrees.

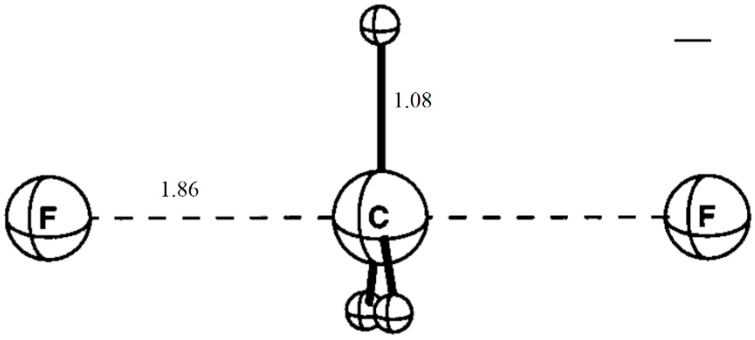

◄Figure 7

Figure 8 ►

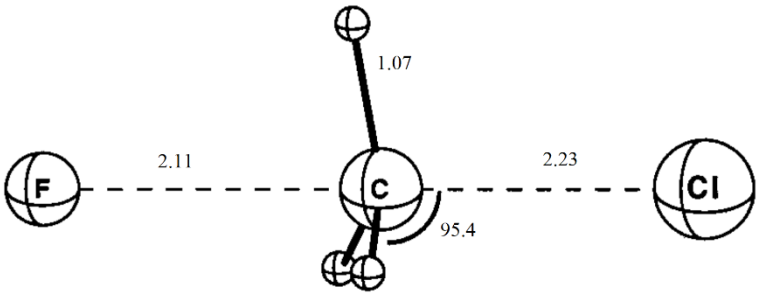

Figure 9 ▶

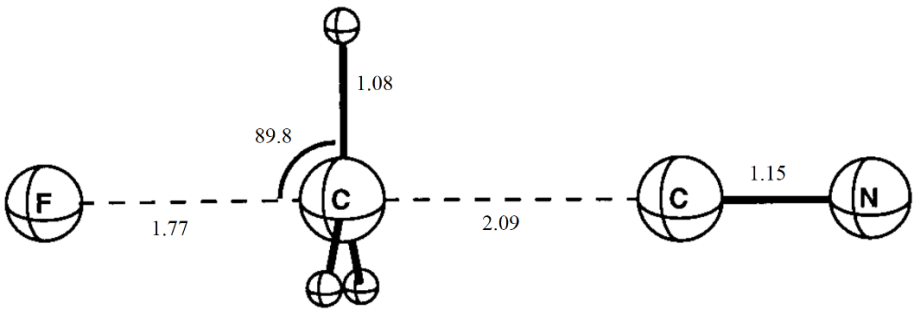

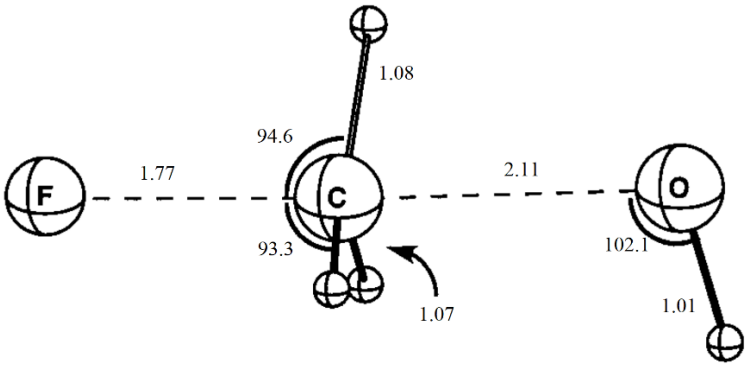

◀Figure 10

Figure 11 ▶

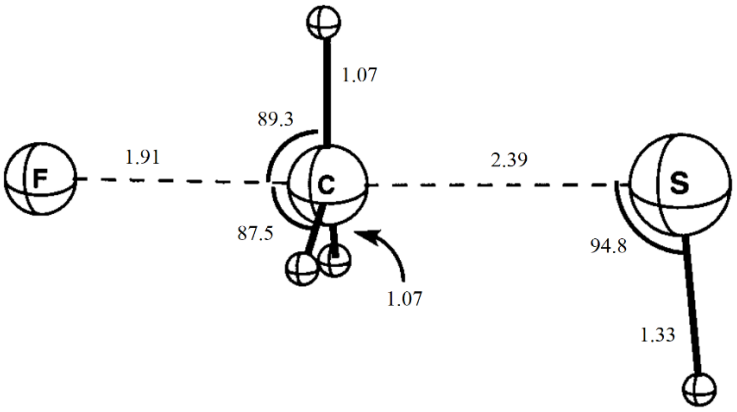

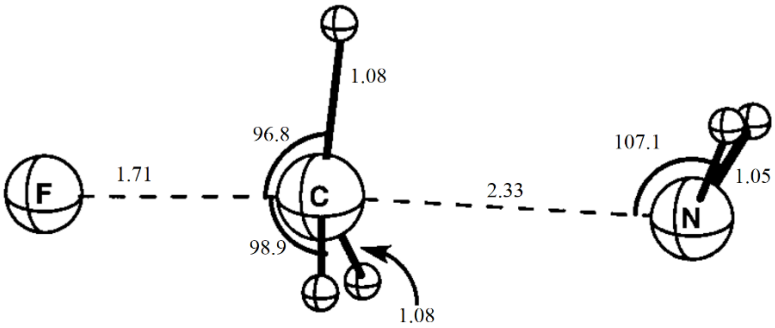

◀Figure 12

The transition state energetics are noted down in Table 8. We also calculated the **forward (E^F)** and **reverse (E^B)** activation energies w.r.t the TS energy.

Table 8: Activation barriers calculated using TS energy

Note: All values are in **Hartree** units.

	E_{reac}	E_{TS}	E_{prod}	E^B	E^F
F	-238.999	-238.979	-238.999	0.020	0.020
Cl	-599.005	-598.994	-599.039	0.011	0.045
CN	-232.003	-231.938	-231.971	0.065	0.032
OH	-215.027	-214.95	-214.965	0.077	0.015
SH	-537.631	-537.564	-537.598	0.066	0.033
NH_2	-195.165	-195.073	-195.084	0.092	0.011

2. IRC Calculations:

The Intrinsic Reaction Coordinate (IRC) [4] calculation gives a unique connection from a given transition structure to local minima of the reactant and product sides. This allows for easy understanding of complicated multistep mechanisms as a set of simple elementary reaction steps.

Mathematically, IRC is the mass-weighted steepest descent path on the potential energy surface (PES), starting from the transition structure (TS), that is, first-order saddle point. IRC gives a unique connection from a given TS to two local minimum structures.

We calculated the forward and backward IRC using the Gaussian software for all the reactions. The results are published graphically below:

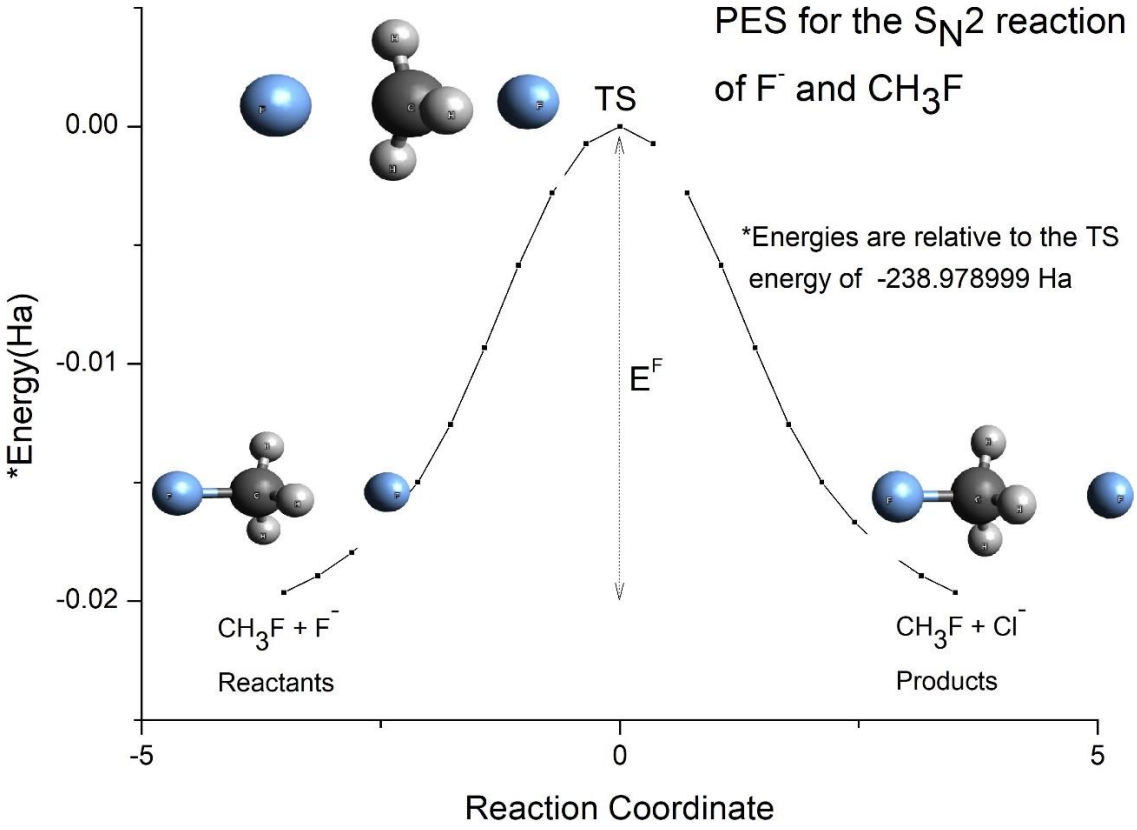

◀Graph 1

Graph 2 ▶

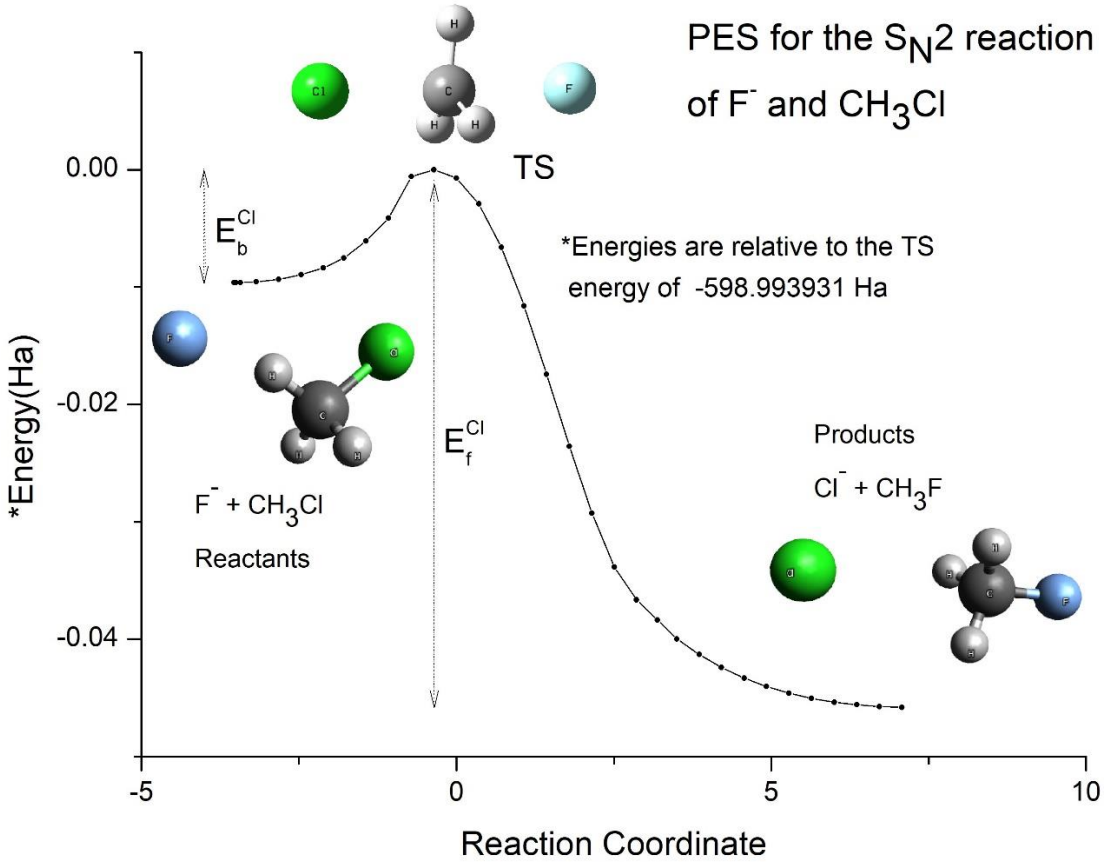

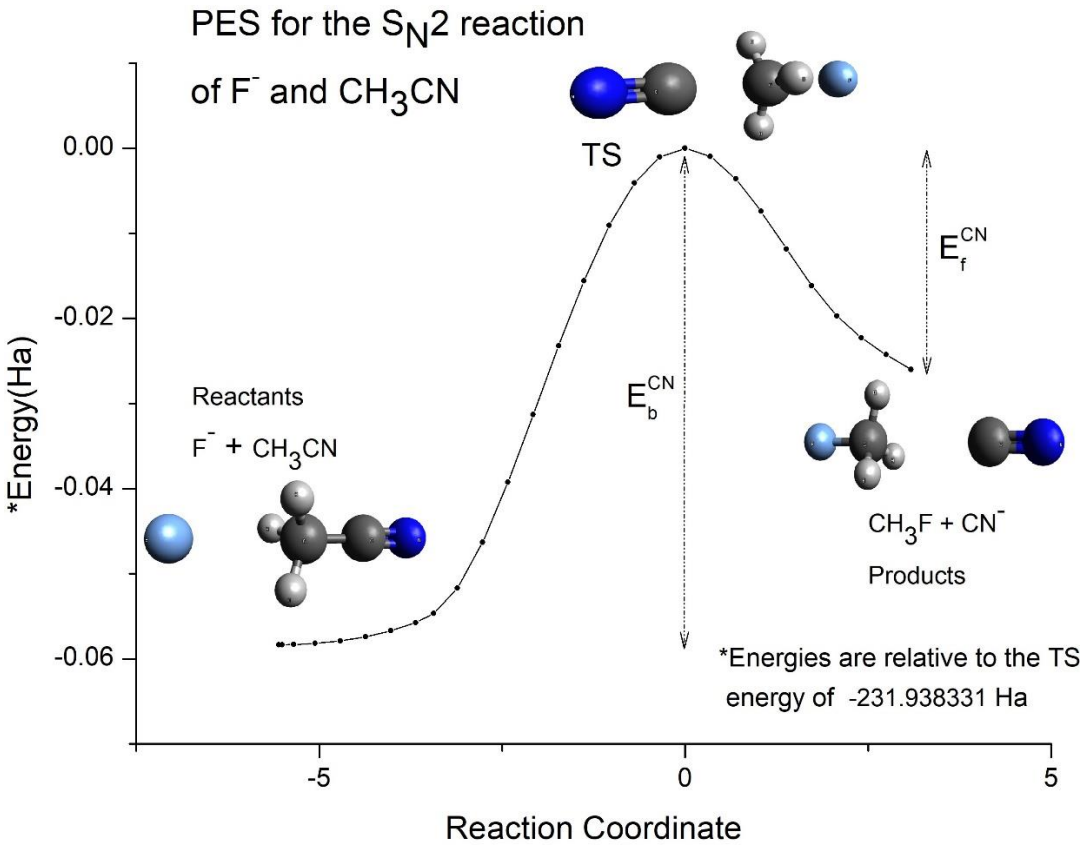

◀Graph 3

Graph 4 ▶

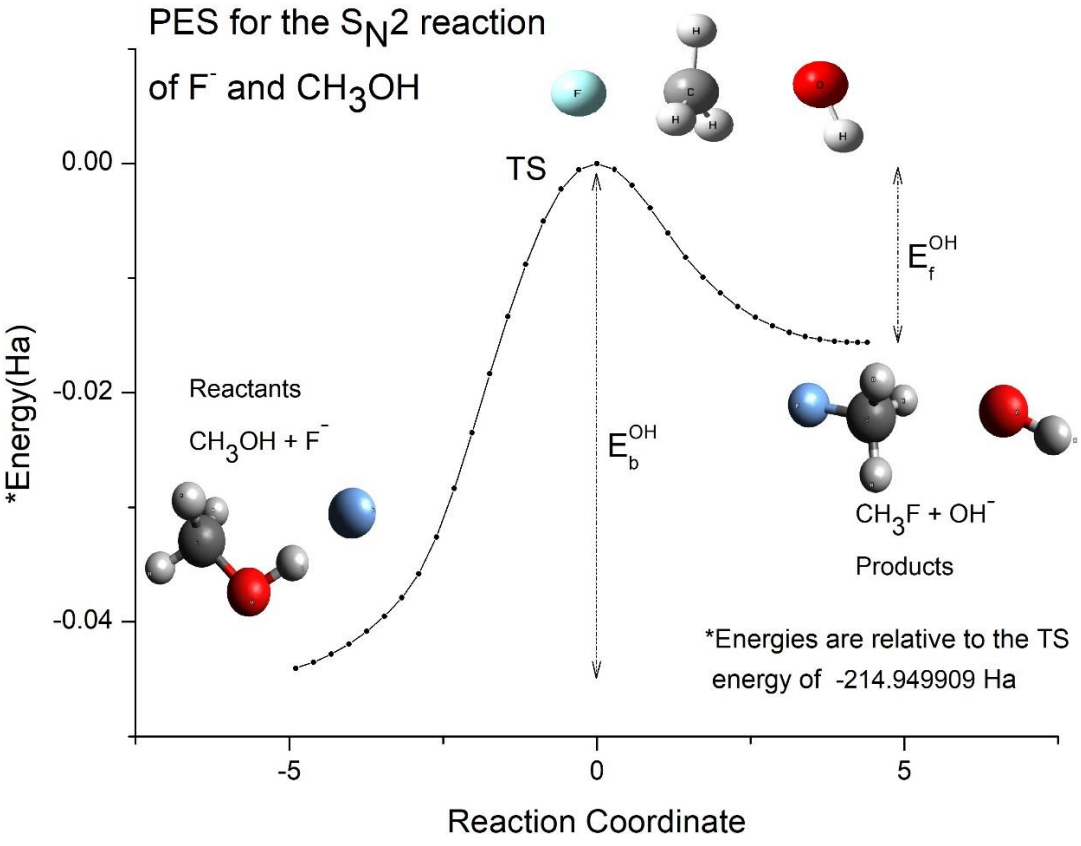

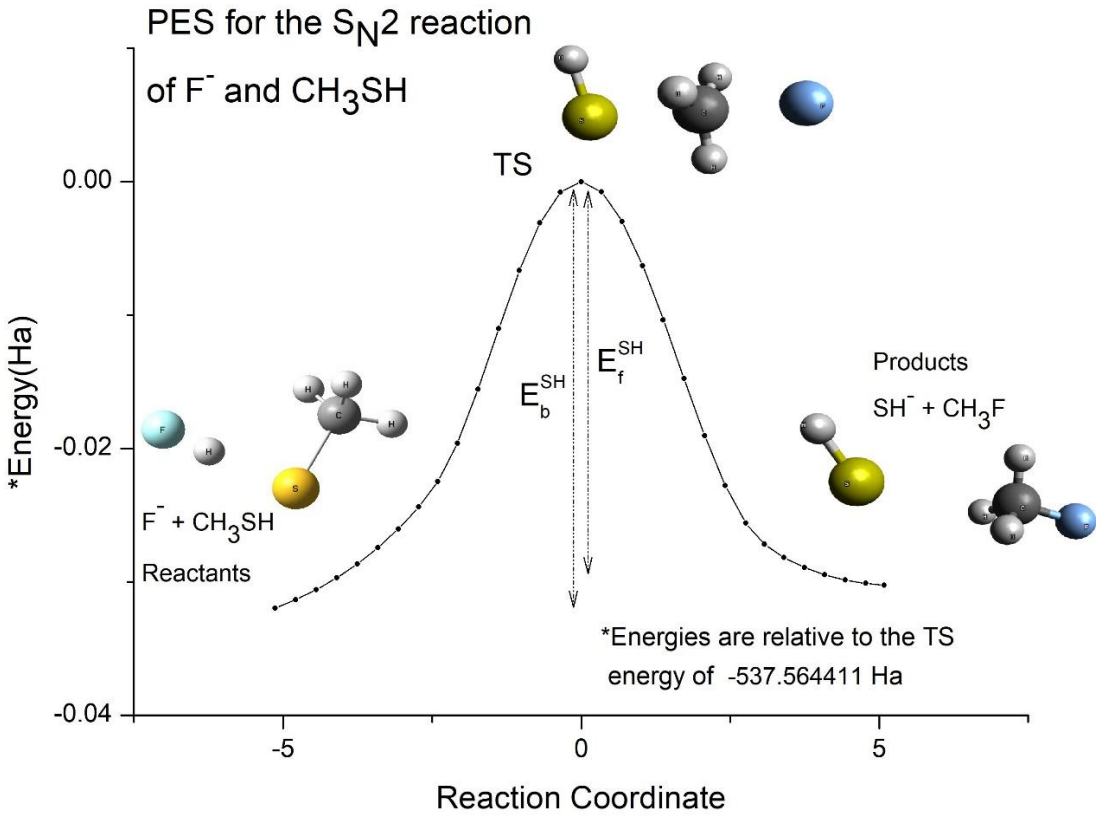

◀Graph 5

Graph 6 ▶

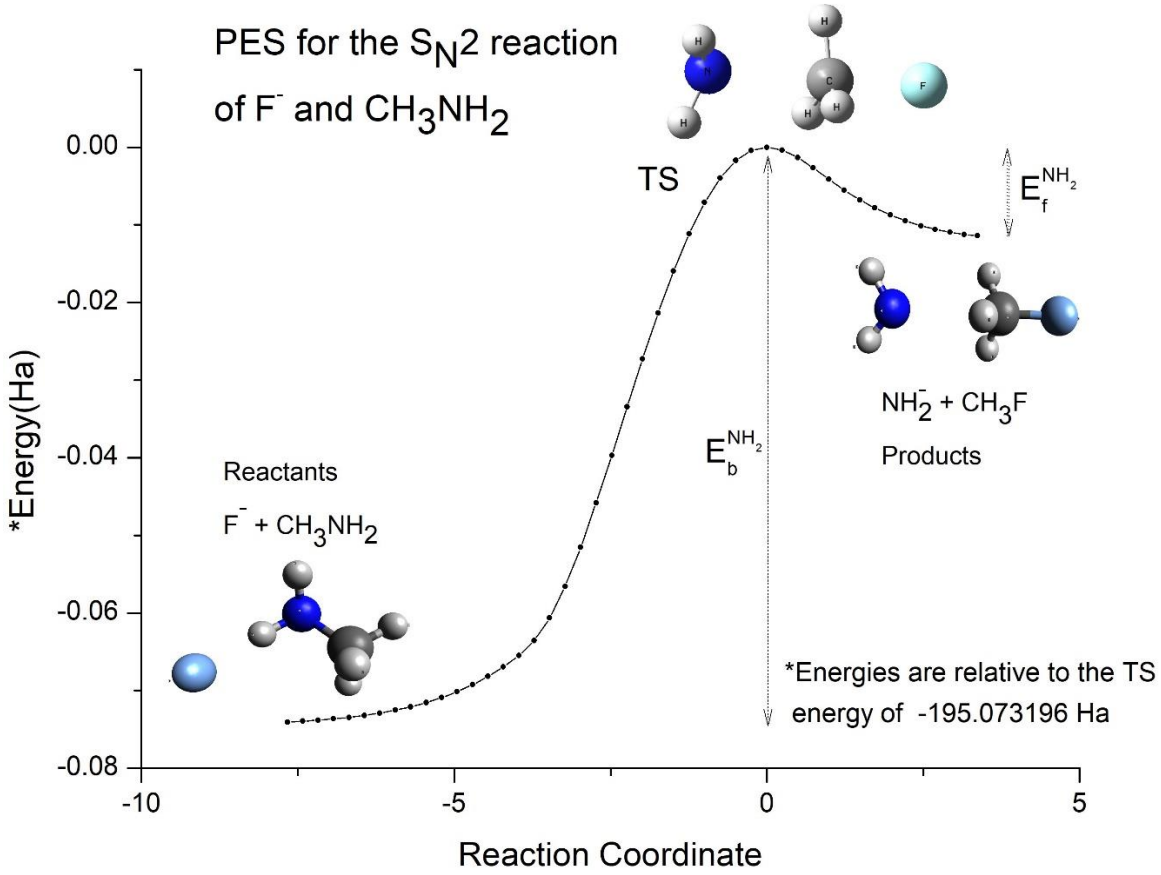

Now we consider the energetics obtained from IRC calculations. The **forward (E^F)** and **reverse (E^B)** activation energies, shown in Table 9, are obtained from the IRC plots.

Table 9: Activation barriers based on IRC calculations

	E^F	E^B
F	0.019	0.019
Cl	0.009	0.045
CN	0.058	0.025
OH	0.044	0.015
SH	0.031	0.030
NH_2	0.060	0.011

Note: All values are in **Hartree** units.

3. Results:

In this section, we summarize the data obtained by TS optimizations and IRC calculations. The resulting predictions are compared to those of coupled cluster singles and doubles theory augmented by a perturbative contribution from connected triple excitations [**CCSD(T)**] [3].

The following Table 10 tabulates the forward and backward barriers obtained by TS and IRC calculations alongside the CCSD(T) values:

Table 10: Comparison of Activation barriers (in kcal mol^{-1}) with CCSD(T) values

	TS BARRIERS		**IRC BARRIERS**		**CCSD(T) VALUES**	
	E^F	E^B	E^F	E^B	E^F	E^B
F	12.82	12.82	12.31	12.31	13.11	13.11
CL	28.75	7.14	28.73	6.04	28.07	5.45
CN	20.65	40.82	16.30	36.60	20.76	38.96

OH	9.84	48.50	9.80	27.64	10.73	47.84
SH	21.19	41.95	18.98	20.05	20.8	41.99
NH_2	7.30	58.07	7.15	38.05	7.11	53.25

Finally, we look at the mean absolute deviations of TS and IRC values about the CCSD(T) data:

Table 11: Mean Absolute Deviations (in kcal mol^{-1}) of TS and IRC energetics with CCSD(T) values

	ABSOLUTE DEVIATION OF TS FROM CCSD(T)		ABSOLUTE DEVIATION OF IRC FROM CCSD(T)	
	δE^F	**δE^B**	**δE^F**	**δE^B**
F	0.284	0.284	0.792	0.792
CL	0.686	1.699	0.669	0.592
CN	0.103	1.861	4.451	2.351
OH	0.886	0.661	0.928	20.192
SH	0.391	0.039	1.818	21.935
NH_2	0.198	4.826	0.043	15.191
MEAN ABSOLUTE DEVIATION	**0.425**	**1.562**	**1.450**	**10.175**

Thus, we notice that the deviations of QST3 calculations from CCSD(T) values are quite low with δE^F = 0.4 and δE^B = 1.5. This shows that QST3 was able to appropriately optimize TS structure from their optimized reactants and products.

On the other hand, for the IRC calculations, we obtained $\delta E^F = 1.4$ and $\delta E^B = 10.1$. We noticed anomalies in the IRC data while working with groups such as OH, SH and NH_2. For them, the deviation in the backward barrier turned out to be quite large. This is probably caused due to the IRC calculations converging before it has reached the "true" reactant/product.

This instability of the IRC may be caused due to the valley-ridge inflection (VRI). The VRI may invoke a bifurcation of a bunch of dynamical trajectories with different initial conditions into one side and the other side of the ridge, through contributions of molecular vibrations perpendicular to the IRC tangent. In such cases, the REAC-TS-PROD connection obtained by the IRC approach can be inaccurate.

- **Conclusions:**

A comprehensive data of electronic structure predictions has been generated and analyzed for the family of S_N2 reactions:

$$CH_3X + F^- \rightarrow CH_3F + X^-, \quad \text{where X= (F, Cl, CN, OH, SH } NH_2).$$

All relevant reactants, products, and transition states, optimized geometries, and relative energies were computed. In this study, HF, MP2 and B3LYP methods were utilized with 6-31+G(d) basis set for geometric structure determinations.

Statistics for the performance of various theoretical methods, with respect to CCSD(T) standards, on the geometric structures of the SN2 reaction profiles appear in Table 7-Table 11. Comparison of experimental gas phase data is done with the computed energetics, which is shown in those tables.

The forward and reverse S_N2 reactions of the $CH_3X + F^-$ systems exhibit diverse energetic and topological features, with scattered energetics and activation barriers. All of the product complexes ($FCH_3.X^-$) are backside and electrostatic in nature, with heavy-atom frameworks more or less linear. The reactant $F^-.CH_3CN$ complex is a distorted backside adduct displaying a hydrogen bond to a single methyl hydrogen. In contrast, the $CH_3X.F^-$;(X = OH, NH_2) reactant complexes are frontside species with a strong, partially covalent bond of F^- to an acidic hydrogen.

Our study shows that backside ion-molecule intermediates do not exist on the reactant side of the $CH_3X.F^-$ potential surfaces for X=OH, SH, NH_2. In these systems we find the intrinsic reaction path (IRP) to circuitously connect the S_N2 transition state to the deep minima of the frontside structures, in which acidic protons are complexed or even abstracted by the fluoride anion. Accordingly, the potential surfaces in these three cases do not fit neatly into the classic double-well picture of Figure 1. In the chemical reaction dynamics of such S_N2 systems, most of the classical trajectories leading from reactants to products are likely to skirt the frontside minima, preferring direct backside attack instead.

- **References:**

1. Gonzales, J., Allen, W. and Schaefer, H., 2005. Model Identity SN2 Reactions CH3X + X- (X = F, Cl, CN, OH, SH, NH2, PH2): Marcus Theory Analyzed. *The Journal of Physical Chemistry A*, 109(46), pp.10613-10628. Available at: <https://pubs.acs.org/doi/10.1021/jp054734f>.
2. Gonzales, J., Cox, R., Brown, S., Allen, W. and Schaefer, H., 2001. Assessment of Density Functional Theory for Model SN2 Reactions: CH3X + F-(X = F, Cl, CN, OH, SH, NH2, PH2). *The Journal of Physical Chemistry A*, 105(50), pp.11327-11346. Available at: <https://pubs.acs.org/doi/10.1021/jp012892a>.
3. Gonzales, J., Pak, C., Cox, R., Allen, W., Schaefer III, H., Császár, A. and Tarczay, G., 2003. Definitive Ab Initio Studies of Model SN2 Reactions CH3X+F (X=F, Cl, CN, OH, SH, NH2, PH2). *Chemistry - A European Journal*, 9(10), pp.2173-2192. Available at: <https://chemistry-europe.onlinelibrary.wiley.com/doi/abs/10.1002/chem.200204408>.
4. Maeda, S., Harabuchi, Y., Ono, Y., Taketsugu, T. and Morokuma, K., 2014. Intrinsic reaction coordinate: Calculation, bifurcation, and automated search. *International Journal of Quantum Chemistry*, 115(5), pp.258-269. Available at: <https://onlinelibrary.wiley.com/doi/full/10.1002/qua.24757>.
5. M. J. Frisch, G. W. Trucks, H. B. Schlegel, G. E. Scuseria, M. A. Robb, et al., *Gaussian 09* (Gaussian, Inc., Wallingford CT, 2009).